An optimized relevant long short-term memory-squared gain extended Kalman filter for the state of charge estimation of lithium-ion batteries.

TAKYI-ANINAKWA, P., WANG, S., ZHANG, H., LI, H., XU, W. and FERNANDEZ, C.

2022

An optimized relevant long short-term memory-squared gain extended Kalman filter for the state of charge estimation of lithium-ion batteries

Paul Takyi-Aninakwa[1], Shunli Wang[1*], Hongying Zhang[1], Huan Li[1], Wenhua Xu[1], Carlos Fernandez[2]

[1]*School of Information Engineering, Southwest University of Science and Technology, Mianyang, 621010, China*

[2]*School of Pharmacy and Life Sciences, Robert Gordon University, Aberdeen AB10-7GJ, UK*

Abstract: Accurate state of charge (SOC) estimation of lithium-ion batteries by the battery management system (BMS) plays a prominent role in ensuring their reliability, safe operation, and acceptable durability in smart devices, electric vehicles, etc. In this paper, the effect of the training and testing working conditions on the accuracy of the SOC using a long short-term memory (LSTM) network is studied through transfer learning. Secondly, a relevant attention mechanism is introduced as a data optimizer for faster training of the LSTM network to establish a relevant LSTM (RLSTM). Finally, the SOCs estimated by the RLSTM are independently input with the working current to an extended Kalman filter (EKF) and a proposed squared gain EKF (SGEKF) method to iteratively denoise and optimize the accuracy of the final SOC under the three complex working conditions. The results show that the SOC estimation accuracy is influenced by the training and testing working conditions using the LSTM network, which provides a technique for accurate SOC estimation. Also, the established RLSTM network is computationally efficient for accurate SOC estimation. Moreover, the proposed hybrid RLSTM-SGEKF model has an overall maximum mean absolute error, mean squared error, root mean squared error, and mean absolute percentage error values of 0.35299%, 0.0017448%, 0.41765%, and 2.34403%, respectively, under the three complex working conditions. The proposed hybrid RLSTM-SGEKF model is optimal, robust, and computationally efficient for accurate SOC estimation of lithium-ion batteries for real-time BMS applications.

Keywords: state of charge; lithium-ion battery; long short-term memory; working condition-based training and testing; relevant attention mechanism; squared gain extended Kalman filter

***Corresponding author**: Shunli Wang; E-mail address: 497420789@qq.com

Nomenclature	
ADAM	Adaptive moment estimate
AEKF	Adaptive extended Kalman filter
Ah	Ampere-hour integral method
BBDST	Beijing bus dynamic stress test
BMS	Battery management system
CC	Constant current
CNN	Convolutional neural network
CPU	Central processing unit
CV	Constant voltage
DEKF	Dual extended Kalman filter

DST	Dynamic stress test
ECM	Equivalent circuit model
EKF	Extended Kalman filter
EM	Electrochemical model
EV	Electric vehicle
HPPC	Hybrid pulse power characterization
MAE	Mean absolute error
LSTM	Long short-term memory
MAPE	Mean absolute percentage error
ME	Maximum error
MSE	Mean squared error
NMC	Nickel manganese cobalt
NN	Neural network
OCV	Open-circuit voltage
PF	Particle filter
PSO	Particle swarm optimization
RLSTM	Relevant long short-term memory
RMSE	Root mean squared error
RNN	Recurrent neural network
SGEKF	Squared gain extended Kalman filter
SOC	State of charge
UKF	Unscented Kalman filter

1. Introduction

Lithium-ion batteries have gradually become the most promising energy storage for smart devices, e-bikes, electric tools, hoverboards, electric vehicles (EVs), etc., compared to other secondary batteries (nickel-cadmium, nickel-metal hydride, and lead-acid batteries) [1–3]. It is due to their appreciable advantages, such as high specific energy, high power densities, high charging rates, low memory effect, low self-discharge rate, longevity, etc. [4, 5]. However, due to the effects of the complex physical, nonlinear electrochemistry, and environmental changes (temperature, humidity, pressure, etc.) during their operations, lithium-ion batteries of the same chemistry have different useful lives in real-time. Therefore, accurate state of charge (SOC) estimation methods that are robust under various working conditions have become essential [6, 7].

The SOC is defined as the ratio of the maximum capacity available for use to the rated capacity of the battery, which is usually expressed as a percentage. The SOC indicators in EVs work similarly to the fuel gauges in internal combustion engine vehicles [8]. With the loss of active materials and lithium-ion inventory, the ability to store energy and provide an optimal power supply degrades, which nonlinearly reflects the decrease in the capacity and increase in internal impedance (resistance and reactance) of the battery [9–11]. Therefore, it is an essential function of the battery management system (BMS) to accurately estimate the SOC of the battery [12, 13]. The BMS is embedded to monitor the working conditions, such as current, voltage, ambient temperatures, self-discharge rates, aging, etc., to accurately determine the SOC, which is critical to ensure the safe, reliable, and stable operation of the lithium-ion battery in real-time applications [14, 15]. An accurate SOC estimation is of great significance because it prevents unexpected system interruptions, over-charge, over-discharge, and ensures the safety of the

battery and its users [16]. Furthermore, it guides users to intuitively determine the state of health and remaining useful life by observing the rate of SOC variations during the charge and discharge states. Due to the high nonlinearities, the SOC value of the battery cannot be measured directly but can be estimated by utilizing measurable battery parameters, such as current, voltage, temperature, etc., due to their strong correlation with the SOC [17].

Charge and discharge control, state estimations, thermal management, fault diagnostics, and safety of lithium-ion batteries have been thoroughly researched [18, 19]. SOC estimation methods can be divided into three categories: direct measurement, model-based, and data-driven methods. The direct measurement methods, such as open-circuit voltage (OCV) [20] and Ampere-hour (Ah) integral [21] methods, are simple and easy to implement for SOC estimation but vulnerable to the battery's state and working conditions. In particular, the Ah integral method significantly accumulates errors during the integration due to variations in the load current measurement. Also, it is highly dependent on the initial SOC value, which might result in large errors [22]. Therefore, this method needs high-precision sensors to obtain an accurate current measurement to overcome this challenge, which is expensive to employ in real-time applications. The OCV method requires a long shelf time for the recovery and accurate measurement of the OCV value of the battery. Also, it strongly relies on accurate voltage measurement, and any error leads to an inaccurate SOC estimation, which makes it practically challenging to apply [23].

For the model-based method, also known as the closed-loop method [24], battery models are established, which are categorized into three kinds: an electrochemical model (EM), an empirical (simplified electrochemical) model, and an equivalent circuit model (ECM), to monitor and simulate the dynamic electrochemistry of the battery [25, 26]. These models measure the operational or real-time parameters of the battery using inputs such as the current, voltage, temperature, etc. [27–29]. For this SOC estimation method, the battery model is usually constructed and expressed as a state-space model for a state observer [30]. Some state observers commonly established are the Kalman filter (KF) [31–33] and its advanced models: extended, adaptive, and dual Kalman filter (EKF/AEKF/DEKF) [34–40], and unscented Kalman filter (UKF) [41–43], particle filter (PF) [44, 45], sliding mode observer [46, 47], and H-infinity observer [48]. Despite their potential, they are highly dependent on the accuracy of the battery model, which is difficult to establish. Also, the accuracy and stability of this method are affected by operational and environmental conditions, which cause the modeling of the voltage characterization to become complicated and result in inaccurate SOC estimation [49, 50]. Furthermore, the high cost and laborious measurement of the internal parameters of the battery with their complex aging characteristics make them difficult to implement in real-time applications [51]. From a theoretical perspective, this estimation method is exclusively based on an understanding of the battery's electrochemical reactions, which have several complex mathematical equations, resulting in difficulties in the construction of the battery model and parameter computation [19].

In recent years, several data-driven methods have served as the most promising methods to overcome the limitations of the other existing methods and have been extensively utilized. Due to their excellent self-adaptation, self-learning, and high performance, neural networks (NNs) have been utilized to estimate the SOC of lithium-ion batteries. This estimation method is model-free, and its performance is highly dependent on the quality and quantity of the input data coupled with proper training skills and the appropriate definition of the hyperparameters [52]. For this method, the battery is considered a "black box" rather than a practical mathematical model, which means fewer computational complexities and variables. It directly models the nonlinear relationships by feature extraction, including the electrochemical reaction, aging processes, self-discharge rates, aging, etc., between its states and the measured variables through an

adequate amount of training and testing data [53–56] without prior knowledge of the system. It seeks to estimate the SOC after learning from a nonlinear battery's data by considering factors such as the ohmic resistance, polarization effects, self-discharge, etc., to achieve high accuracy, which is more reliable than other estimation methods. It is unlike the model-based method, where these factors have to be particularly considered in the established battery model and state observer for the estimation.

Commonly used NNs for SOC estimation include artificial, backpropagation, recurrent neural network (RNN) [57–59], gated recurrent units [60], long short-term memory (LSTM), and nonlinear autoregressive with exogenous input networks [61, 62], etc. Bian et al. [63] established a stacked bidirectional LSTM network for SOC estimation of lithium-ion batteries. However, its computational complexity and structure add up to the long training time of the LSTM network. Also, the estimation results have noise, and the accuracy needs to be improved. Almaita et al. [64] used the LSTM for SOC estimation and compared its performance with that of the feed-forward neural network (FFNN) and a deep FFNN. The estimation results show that LSTM is more optimal compared to the other networks by having a root mean square error (RMSE) of 6.9539%, which needs to be improved. Xi et al. [65] constructed a SOC estimation method using a time-delayed RNN and LSTM through the identification of the root cause of unexpected poor performances using overexcited neurons. The estimation results show that both networks do not have a good track of the actual SOC but have high noise effects.

In the above studies, only the LSTM network was employed, which has limitations that affect its accuracy, robustness, and training time. When it comes to the LSTM network, when it is not optimized during its training, a hybrid method is employed instead, which has proven to give optimal estimation performance. The SOC estimation method using data-driven and model-based methods can be classified as a hybrid method. This method has proven to have optimal accuracy compared to the traditional network to overcome the inherent limitations of the LSTM for better SOC estimation performance of lithium-ion batteries [66, 67]. Song et al. [68] proposed a hybrid convolutional neural network (CNN)-LSTM network to estimate the battery SOC. The estimation results show that the RMSE and mean absolute error (MAE) values are 1.31% and 0.92%, respectively. Yang et al. [69] proposed a slow-trained LSTM-RNN network for the sophisticated battery behaviors and used the traditional UKF as the noise filter and optimization method. Fasahat et al. [70] proposed a hybrid autoencoder neural network and an LSTM network for the SOC estimation of lithium-ion batteries. It is observed that their method estimates MAE and RMSE values of 0.63% and 0.90%, respectively. Shin et al. [71] estimated SOC based on the EKF is proposed in which the errors are compensated using the slow-trained LSTM network, which estimates an average error value of 0.80%. Ren et al. [72] proposed a hybrid particle swarm optimization (PSO)-LSTM network for the SOC estimation under noise characterization. The estimation results show that the hybrid PSO-LSTM network has maximum error (ME) values of 2.49% and 3.14%, while the LSTM network estimates an ME value of 3.92% and 1.76% with and without noise, respectively.

Generally, the results estimated by these hybrid models need improvement for a more satisfactory and accurate characterization of the SOC of lithium-ion batteries in terms of robustness, optimal adaptability to training and testing conditions, and multiple model choices. Working conditions such as the Beijing bus dynamic stress test (BBDST), dynamic stress test (DST), hybrid pulse power characterization (HPPC), etc., used for training and testing of the SOC exhibit different current, voltage, temperature, energy, etc., characteristics for the charge and discharge states. The characteristic effects of these working conditions on the training and testing using the traditional LSTM network to determine the influence of the SOC estimation accuracy have not been investigated. Therefore, understanding the effect of working conditions

(dataset profiles) on the SOC estimation accuracy of lithium-ion batteries can play a significant role in the optimal design, training, and testing using networks.

In this paper, the effect of training and testing an LSTM network using different complex working condition profiles on the accuracy of the SOC is studied through a transfer learning technique. The training and testing are conducted under the BBDST, DST, and HPPC working conditions using different experimental datasets and characteristic time cycles to reflect various phenomena. The major contributions of this paper are in five folds:

(1) An LSTM network is trained and tested based on working conditions with different charging and discharging characteristics to study their effects on the accuracy of the SOC estimation. The training and testing are conducted based on an established sequence presented in this paper.

(2) A relevant attention mechanism is introduced as a data optimizer to establish a relevant LSTM (RLSTM). It extracts the relevant features from the training dataset to train the network with highly reduced training time and computation iterations to achieve accurate and efficient SOC. The LSTM and RLSTM networks are trained using an adaptive moment estimate (ADAM), which is computationally efficient and requires low memory.

(3) The SOCs estimated by the RLSTM are independently input with the working current to the EKF and a proposed squared gain EKF (SGEKF) method to denoise and further optimize the accuracy of the final SOC.

(4) The performance evaluation and verification of the working condition-based trained and tested LSTM network, the proposed RLSTM, RLSTM-EKF, and RLSTM-SGEKF models are evaluated using the MAE, RMSE, mean square error (MSE), and mean absolute percentage error (MAPE) metrics to show their accuracy and robustness for SOC estimation compared to other existing methods.

(5) Finally, the final results show that the proposed working condition-based training and testing technique provides a criterion for accurate SOC estimation. Furthermore, the proposed hybrid RLSTM-EKF and RLSTM-SGEKF models have more accurate SOC estimation performance than the LSTM and RLSTM networks. However, the optimized hybrid model, RLSTM-SGEKF, has three (3) times faster estimation speed and better initialization than the RLSTM-EKF model. It solves the convergence and speed issues essential in the SOC estimation of lithium-ion batteries to show its suitability, robustness, and efficacy for the real-time BMS application due to its low computational requirements.

The remaining sections of this paper are organized as follows: Section 2 introduces the mathematical analysis: the architecture of the LSTM network; the working principle of the relevant attention mechanism and hyperparameter selection for the LSTM and RLSTM networks; the working principle of the EKF and SGEKF methods; the flowchart of the models for SOC estimation; and the performance evaluation metrics. Section 3 describes the experimental analysis: the experimental test platform and procedures, the SOC estimation results, and the performance evaluation of the models. Section 4 is the conclusion of this paper.

2. Mathematical analysis

2.1 *The architecture of the LSTM network*

The extension of the FFNN is the RNN. However, the RNN has a short-term memory problem and cannot solve long-term dependencies for time-series predictions. Also, due to the weight effect of the transition matrix associated with the neurons during the backpropagation through time and layers, the gradient either explodes (tends to infinity) or vanishes (tends to zero) during its training process [73, 74]. Through a gating mechanism called the memory cell, the LSTM precisely models chronological sequences and long-term dependencies with its encoder connections. The memory cell and forgetting

modes enable the LSTM network to achieve more accurate SOC estimation and other prediction studies by flexibly adapting to arbitrary timing features during the training of the network [75]. The three gates of the LSTM network are a forget gate f_t, an input gate i_t, and an output gate o_t to protect and control the memory cell.

The forget gate f_t determines which information from the current input data x_t and hidden state h_{t-1} of the previous LSTM cell should be stored or discarded through the sigmoid layer by directing each information input to either 1 or 0, respectively. The mathematical expression for the forget gate is presented in Eq. (1).

$$f_t = \sigma_s * (w_f * [x_t, h_{t-1}] + b_f) \tag{1}$$

The input gate i_t (cell status update) decides which new information should be stored in the memory cell. It receives the information from the current input data x_t and the previous hidden state h_{t-1} and passes it through the sigmoid and *tanh* layers. Firstly, the sigmoid layer decides which new information is contained in the current input x_t that should be used to update the cell. Secondly, the *tanh* layer creates a cell state vector $\tilde{C}_t$ for new information, which is added to the cell state. These two layers work together to decide the information that should be stored in the cell state, as presented in Eq. (2).

$$\begin{cases} i_t = \sigma_s * (w_i * [x_t, h_{t-1}] + b_i) \\ \tilde{C}_t = tanh * (w_c * [x_t, h_{t-1}] + b_c) \end{cases} \tag{2}$$

Then, an addition to the point-wise multiplication of the input gate i_t and the cell state vector $\tilde{C}_t$ is established to update the memory cell for a current cell state C_t. The output information of the forget gate f_t and the previous cell state C_{t-1} are multiplied, as presented in Eq. (3).

$$C_t = f_t * C_{t-1} + i_t * \tilde{C}_t \tag{3}$$

The output gate o_t determines the information for the next hidden state h_{t+1} based on filtered information from the current cell state C_t. Firstly, the sigmoid layer determines which information in the memory cell state to output. Secondly, the *tanh* layer controls the information from the current cell state C_t between –1 and 1. Then, it is multiplied by the output o_t of the sigmoid layer to get the current hidden state h_t. The mathematical expression for the output gate o_t. The new hidden state h_t is presented in Eq. (4).

$$\begin{cases} o_t = \sigma_s * (w_o * [x_t, h_{t-1}] + b_o) \\ h_t = o_t * tanh * (C_t) \end{cases} \tag{4}$$

From the output gate, the new hidden state h_{t+1}in the current time step is either carried on to be the previous hidden state in the next time step h_{t-1} or used for the estimation.

In Eqs. (1)–(4), σ_s is the sigmoid layer, which helps the LSTM network to either discard or update information by closely directing it to 0 and 1, respectively. Also, x_t is the input in the current time step t, and h_{t-1} is the hidden state or output from the previous time step $t-1$. The *tanh* is the hyperbolic tangent function that controls the information flowing through the network between –1 and 1 to avoid fading. Each gate of the network has a weight w_f, w_i, w_c, and w_o and bias vector b_f, b_i, b_c, and b_o for the forget gate, input gate, memory cell, and output gate, respectively, to enhance the flexibility it to strongly adapt to the training data.

2.2 *The working principle of the relevant attention mechanism and hyperparameter selection*

This paper employs the relevant attention mechanism as a data optimizer to select the relevant inherent features from a piece of information to overcome the inherent overfitting and long training time

of the traditional LSTM network. It optimizes the training of the LSTM network to adaptively select the relevant inherent features from the dataset based on the attention weight attached to the input x_t. It merges the new features based on attention weights [7, 76] to train the traditional LSTM as the RLSTM network with a minimized number of iterations.

The relevant attention mechanism is integrated into the encoder and decoder layers for space and time dimensions. It acquires the context dependency to select relevant features while seeking to eliminate over-reliance on the long-term sequence dependency. The attention mechanism for the *n*-dimensional feature sequence x_t^n in the input sequence x_t is established based on the hidden state h_{t-1}. The cell state of the encoder layer's attention weight a_t at time step t is expressed in Eq. (5).

$$\begin{aligned} a_t^n &= L_e^T * tanh * (w_e * [h_{t-1}, C_{t-1}] + z_e * x^n + b_e) \\ e_t^n &= softmax(\alpha_t^n) = \frac{\exp(\alpha_t^n)}{\sum_{t=1}^{n} \exp(\alpha_t^n)} \end{aligned} \tag{5}$$

In Eq. (5), L_e, $b_e \in \mathbb{R}^T$, $w_e \in \mathbb{R}^{T \times 2h}$, and $z_e \in \mathbb{R}^{T \times T}$ are the features of the input that are learned by the model. The hidden states and cell states of the encoder layer are $h_{t-1} \in \mathbb{R}^h$ and $C_t \in \mathbb{R}^h$, respectively. *H* is the size of the hidden layer, and *n* is the number of sequences in the input data.

After the feedforward propagation is completed, the features with different levels of significance are extracted during the training process. The significance level is reflected by the different weights of Z_e obtained after each feature of the training data. Since the hidden state h_{t-1} and cell state C_{t-1} of the previous time step are input into the relevant attention mechanism, the features also have timing dependence. After obtaining a_t^n, it is normalized by the sigmoid layer to ensure that the sum of attention weights is 1 in this paper. For the input x_t at each time step, a certain attention weight e_t^n is assigned to each of the features to measure the significance of the *n*-dimensional feature at each time step. The output of the first stage attention-weighted $\tilde{x}_t$ is expressed, as presented in Eq. (6).

$$\tilde{x}_t = (e_t^1 x_t^1, e_t^2 x_t^2, \ldots, e_t^n x_t^n)^T \tag{6}$$

Therefore, $\tilde{x}_t$ is used instead of x_t and entered into the encoder layer for the LSTM network, as presented in Eq. (7).

$$h_t = f_1 * (h_{t-1}, \tilde{x}_t) \tag{7}$$

The encoder layer focuses on the relevant features instead of treating all the input data features equally. The second attention layer selectively focuses on the timing difference between the input features. In a model that produces a hidden state h_t, it evaluates a weight vector m_t as the weighted mean, as presented in Eq. (8).

$$m_t = tanh * (w_d * [h_t, s_{t-1}] + b_d) \tag{8}$$

In Eq. (8), w_d and b_d are the weight and bias vectors, respectively. The attention probability β_t of the input sequence at each time is obtained, as presented in Eq. (9).

$$\beta_t = \frac{\exp(m_t^n)}{\sum_{t=1}^{n} \exp(m_t^n)} \tag{9}$$

The assigned weight by the hidden state at different time steps results in the context vector x_t. Therefore, the x_t at time step t is weighted and summed, as presented in Eq. (10).

$$x_t = \sum_{t=1}^{n} \beta_t h_t \tag{10}$$

The attention mechanism is implemented in the decoder layer, where the inherent time dependencies between hidden states at different time steps are learned. The information weighted by the optimizer is used for the SOC estimation. It enables the RLSTM network to train at reduced computation iterations with short path length and time for more accurate SOC estimates than the traditional LSTM network.

Furthermore, in this paper, a stochastic gradient optimizer, the ADAM, is used as a default training optimizer due to its computational efficiency with little tuning and low memory requirements. It is also invariant to gradient diagonal rescaling and is appropriate for SOC estimation with large datasets and nonlinear systems. The ADAM optimizer is used to train both the LSTM and RLSTM networks to minimize the total loss, which updates the network's weights and biases based on the gradient of the loss function in the forward and backward passes until a convergence criterion is achieved [77, 78]. The gradient (β_1) and squared gradient (β_2) decay rates are defined as 0.9 and 0.999, respectively, with a learning rate of 0.01 and a gradient threshold of 1.

2.3 *The EKF and SGEKF methods*

The traditional EKF method applies partial derivatives and first-order Taylor series expansion to the system's inputs to estimate the nonlinearities in the SOC estimation [79, 80]. It estimates the next state $t+1$ based on the measurement of the previous time step $t-1$ and the current time step t of the weight adjustment factor provided by the Kalman gain. The Kalman gain determines how much of the previous and current state measurements (residual) contribute to updating the posteriori state estimate.

In this paper, the Kalman gain is squared to recursively optimize its weight adjustment during the posteriori state estimate of the measurement update step to ensure a more accurate, denoised, and stable SOC estimation, as presented in Eq. (11).

$$\hat{x}_t^+ = \hat{x}_t^- + K_t^2 * (y_t - \hat{y}_t) \tag{11}$$

In Eq. (11), $\hat{x}_t^+$ and $\hat{x}_t^-$ are the posteriori and priori state estimates, respectively. y_t and $\hat{y}_t$ are the priori and posteriori state measurements, respectively. K_t is the Kalman gain, which is the weight adjustment factor for the two measurements is squared in this paper to establish the SGEKF method. Meanwhile, all the other working steps of the traditional EKF remain unchanged.

The SOC is the ratio of the remaining capacity or energy to the rated capacity of the lithium-ion battery, which is usually expressed in terms of percentage, as presented in Eq. (12).

$$\begin{cases} SOC_t = 1 - DOD_t = \dfrac{Q}{Q_n} \times 100\% \\ SOC_t = SOC_0 - \dfrac{\int_0^t \eta I(t)dt}{Q_n} \end{cases} \tag{12}$$

In Eq. (12), SOC_t is the current SOC estimated, and DOD_t is the depth of discharge at time step t, where Coulombic efficiency and self-discharge are neglected. Q is the remaining capacity or energy measured and Q_n is the rated capacity of the battery, which may vary from the actual capacity of the battery due to aging and cyclic effects. SOC_0 is the initial SOC when the estimation process begins, η is the Coulombic efficiency, which is defined as 1, and $I(t)$ is the working current at time step t.

2.4 *The LSTM network and the proposed RLSTM, RLSTM-EKF, and RLSTM-SGEKF models for SOC estimation*

For the SOC estimation, the input vectors are $SOC_t = [I_t; V_t]$, where I_t and V_t are the current and voltage values of the lithium-ion battery measured at each time step, respectively. When estimating SOC,

two features are essential: dimensional and transient features. The dimensional feature is related to the current input of the battery data. The transient feature corresponds to the relationship between the previous and current SOC inputs of the battery [68].

The LSTM and RLSTM networks extract the relevant features from the input of the training dataset. Then, the SOC estimated by the RLSTM is input into the EKF and SGEKF models independently with the testing and working current datasets, which denoise the nonlinearities and optimize them for the final SOC. The flowchart for the LSTM, RLSTM, RLSTM-EKF, and RLSTM-SGEKF models for SOC estimation is presented in Fig. 1.

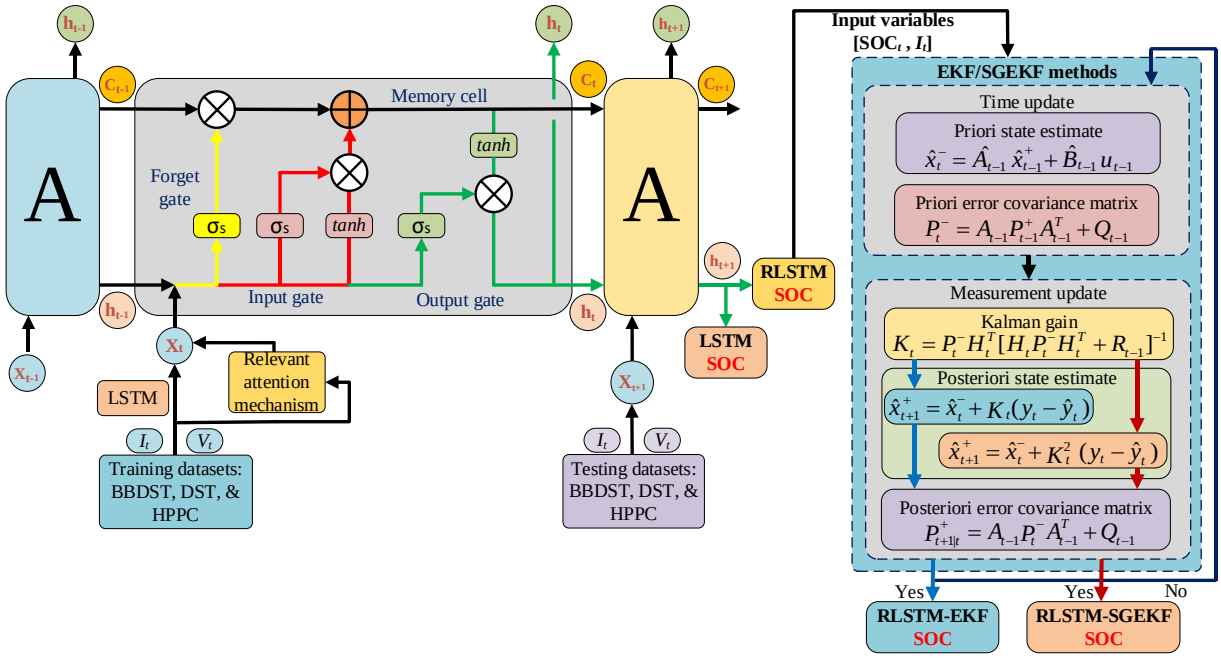

Fig. 1. The flowchart of the LSTM, RLSTM, RLSTM-EKF, and RLSTM-SGEKF models

2.5 *Performance evaluation metrics for the LSTM, RLSTM, RLSTM-EKF, and RLSTM-SGEKF models*

In this paper, to critically study the effect of the working condition-based training and testing on the SOC estimation accuracy of the LSTM network, the error metrics are employed, which are the MAE, RMSE, MSE, and MAPE. These metrics are also used to evaluate the performance of the proposed RLSTM, RLSTM-EKF, and RLSTM-SGEKF models. The mathematical expressions for the metrics are presented in Eq. (13).

$$\begin{cases} E_t = y_t - \hat{y}_t \\ ME = max_t 1,2,\dots,n|E_t| \\ MAE = \frac{1}{n}\sum_{t=1}^{n}|y_t - \hat{y}_t| \\ MSE = \frac{1}{n}\sum_{t=1}^{n}(y_t - \hat{y}_t)^2 \\ RMSE = \sqrt{\frac{1}{n}\sum_{t=1}^{n}(y_t - \hat{y}_t)^2} \\ MAPE = \frac{100\%}{n}\sum_{t=1}^{n}\left|\frac{y_t - \hat{y}_t}{y_t}\right| \end{cases} \quad (13)$$

In Eq. (13), t is the number of non-missing data steps, n is the total number of data points in the sample, and E_t is the estimated SOC error at time step k. y_t is the actual SOC of the battery system and $\hat{y}_t$ is the estimated SOC value using the proposed models. The ME is the absolute maximum error value error in the data sequence. The MAE means that all the individual differences (positive and negative values) are weighted equally in the average value. The MSE is the average of the square of each error value at the time step t. The RMSE shows how dispersed the error is away from the mean. The MAPE is the mean absolute percentage error of the estimated SOC from the actual SOC.

3. Experimental analysis

3.1 *Experimental test platform and procedures*

An NMC70Ah (nickel manganese cobalt oxide) lithium-ion battery is used for the experiments. It has a rated voltage of 4.4 V and a rated capacity of 70 Ah. It has nickel manganese cobalt as the cathode electrode and natural graphitic carbon with metallic backing as the anode electrode. The basic technical specifications of the battery are presented in Table 1.

Table 1. Basic technical specifications of the lithium-ion battery (NMC70Ah)

Parameter	Value	Parameter	Value
Nominal capacity	70 Ah	Standard current	70 A
Nominal voltage	3.7 V	Maximum cut-off current	100 A
Maximum cut-off voltage	4.5±0.05 V	Minimum cut-off current	100 A
Minimum cut-off voltage	2.5±0.05 V	Dimensions: l×w×h	148×33×93 (mm)

For the battery test, a Neware battery test system (CT-4016) is used. It has a maximum current of 100 A, a range of charge and discharge voltage of 25~100 V, and a maximum charge and discharge power of

12 kW. The temperature testing equipment is a DGBELL BTT-331C model, which keeps an ambient temperature of 25 °C throughout the tests. The experimental test platform is presented in Fig. 2.

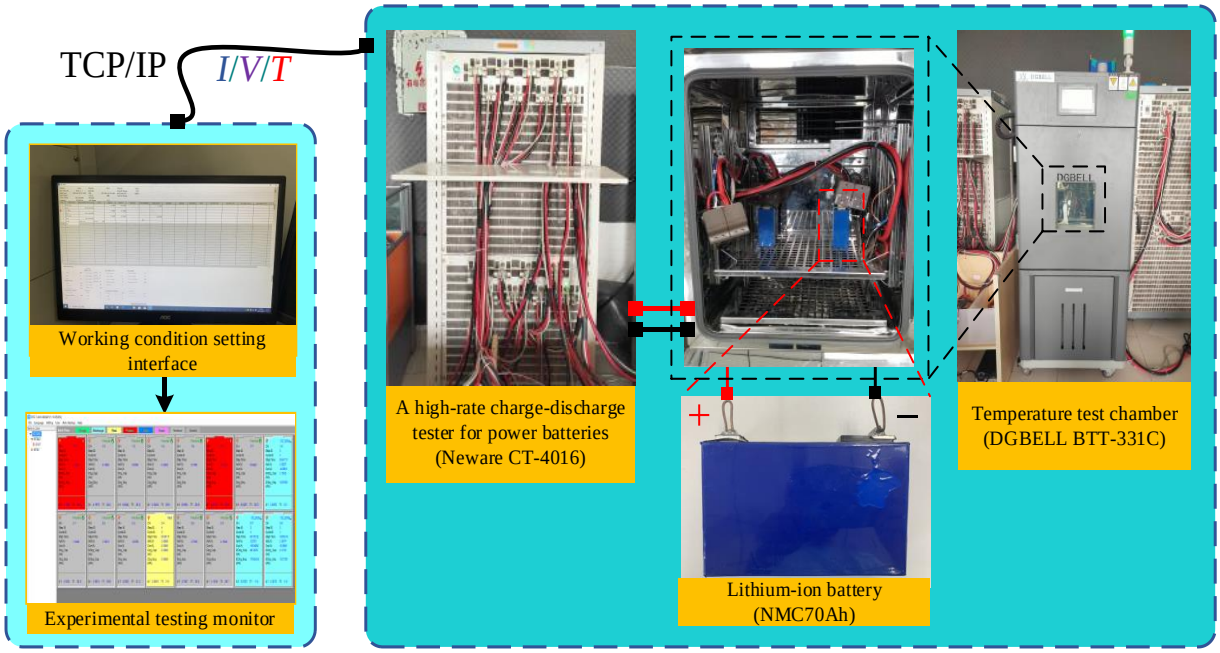

Fig. 2. Experimental test platform

Fig. 2 shows the experimental testing platform established to obtain the charge-discharge characteristics of the lithium-ion battery, such as the current and terminal voltage, for all working conditions. The platform mainly consists of a charge-discharge control circuit, a circuit measurement system, a signal detector, electronic load, temperature test equipment, a direct current power supply to the battery, and a computer for the setting and monitoring of the test steps. The essence of this experimental platform is to obtain the charge-discharge characteristics (current, voltage, capacity, energy, etc.) of the lithium-ion battery for the defined working condition. The battery data for each programmed working condition is stored during the experiment. Firstly, the computer is used to input and send working step commands for the selected working condition through the electronic load of the serial port, which are the charging, discharging, and rest time steps. During the test, the defined steps are switched between the charging, discharging, and resting stages at the predefined step time and can be monitored to know the status and performance of the test. Meanwhile, the current, voltage, and other data are retrieved in real-time using the peripheral inter-connected data acquisition cable. Finally, the current and voltage data are processed, and the charged and discharged state results are graphically displayed by the general-purpose computer and stored.

3.2 *BBDST, DST, and HPPC working conditions*

(a) *BBDST working condition*

The experimental data of the BBDST working condition is obtained by processing the data retrieved from the start, acceleration, slide, brake, rapid acceleration, and stop of the Beijing bus for the lithium-ion battery. In a real-time application, the power of each step is reduced to simulate the Beijing bus's working condition. The complex working steps of the Beijing bus are presented in Table 2.

Table 2. The complex working steps of the Beijing bus

Step	P_c (W)	Step time (s)	Total time (s)	Working status
1	37.5	21	21	Start
2	72.5	12	33	Acceleration
3	4.5	16	49	Slide
4	-15	6	55	Brake
5	37.5	21	76	Acceleration
6	4.5	16	92	Slide
7	-15	6	98	Brake
8	72.5	9	107	Acceleration
9	92.5	6	113	Rapid acceleration
10	37.5	21	134	Acceleration
11	4.5	16	150	Slide
12	-15	6	156	Brake
13	72.5	9	165	Acceleration
14	92.5	6	171	Rapid acceleration
15	37.5	21	192	Acceleration
16	4.5	16	208	Slide
17	-35	9	217	Brake
18	-15	6	229	Brake
19	4.5	71	300	Stop

Assuming the charging is negative and the discharging is positive, the current and terminal voltage curves under the BBDST working condition used for testing the networks are presented in Fig. 3.

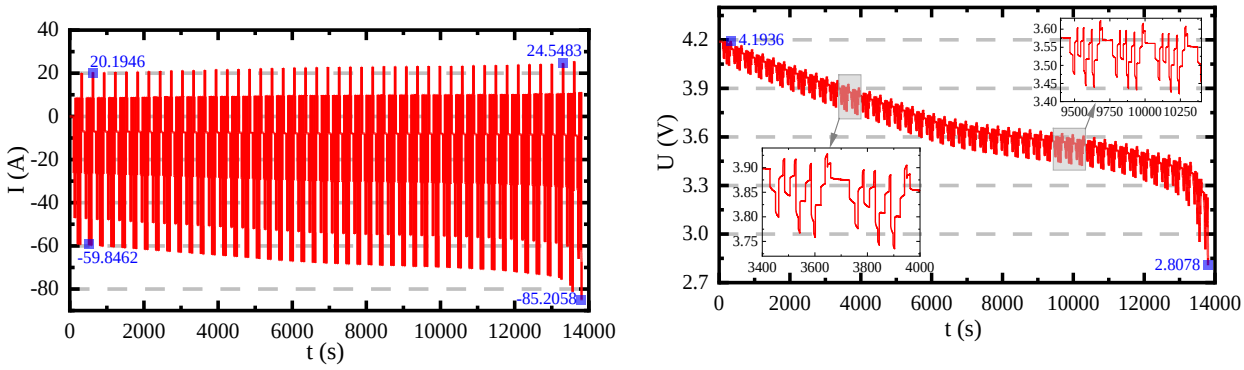

(a) Current variation curve **(b)** Voltage variation curve

Fig. 3. The current and voltage variation curves under the BBDST working condition

(b) *DST working condition*

As a complex working condition, the DST is self-defined. The experimental data (current and voltage) from the DST is used to test the network for SOC estimation of lithium-ion batteries. The experimental test procedures of the DST are described as follows:

(i) The battery is charged to a maximum terminal voltage of 4.20 V with a constant current (CC) of 1 C. Then, it is charged with a constant voltage (CV) until the current rate drops to 0.5 C.

(ii) After charging is completed, the battery is rested to ensure thermal and electrochemical equilibrium before the next test profile for 30 minutes.

(iii) A CC discharge is carried out at a rate of 0.5 C for 4 minutes. Then, the battery is rested for 30 seconds after the discharge.

(iv) The lithium-ion battery is charged at a CC rate of 0.5 C for 2 minutes and rested for 30 seconds.

(v) A CC discharge is performed at a rate of 1 C for 4 minutes.

Steps (iv) and (v) are repeated until the minimum discharge terminal voltage is reached.

Assuming the charging is negative and the discharging is positive, the current and voltage variation curves under the DST working condition used for testing the networks are presented in Fig. 4.

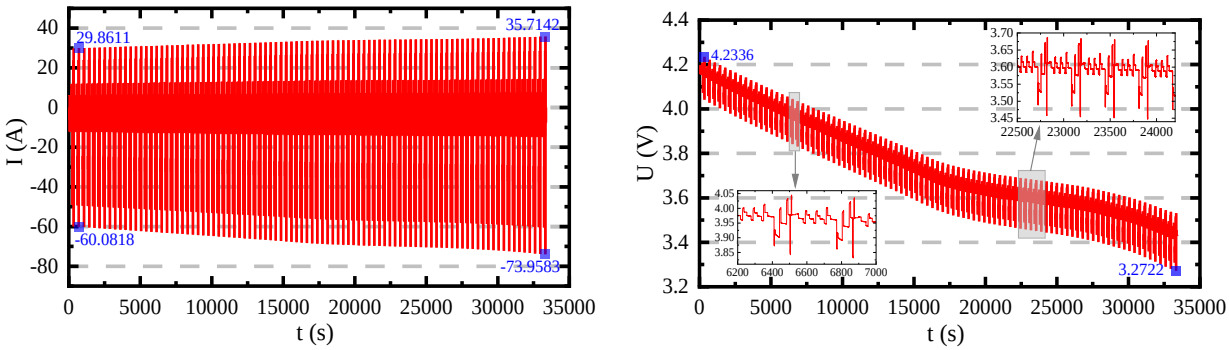

(a) Current variation curve **(b)** Voltage variation curve

Fig. 4. The current and voltage variation curves under the DST working condition

(c) *HPPC working condition*

The HPPC test measures the pulse capability of lithium-ion batteries under varying sequential DOD levels at different time intervals. During the test, the battery is first charged with a 1 C/70, a CC and CV. Then the battery is rested for 40 minutes to ensure electrochemical and thermal equilibrium before the next test profile. A 10-second discharge pulse is applied using a 1 C current rate and rested for 40 seconds. A 10-second charge pulse is initiated at a 1 C current rate and rested afterward for 40 seconds. The next cyclic HPPC is conducted on the lithium-ion battery after a 6-hour rest period. The ten (10) SOC levels are obtained from 0.1 to 1.0 at an interval of 0.1. The corresponding open-circuit voltage for each SOC level is accurately measured before the start of the next HPPC test profile by the test system.

Assuming the charging is negative and the discharging is positive, the corresponding current and terminal voltage curves under the HPPC working condition used for testing the networks are presented in Fig. 5.

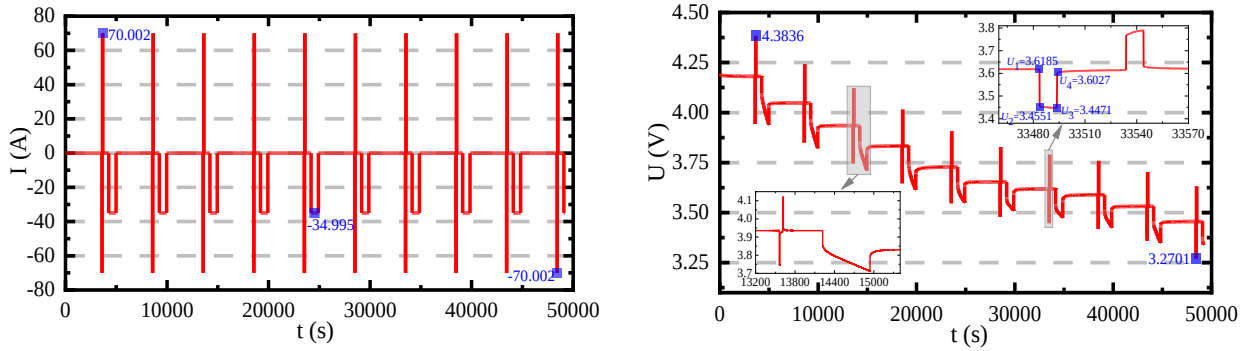

(a) Current variation curve **(b)** Voltage variation curve

Fig. 5. The current and voltage variation curves under the HPPC working condition

3.3 *SOC estimation and performance evaluation for working condition-based training and testing using the LSTM, RLSTM, RLSTM-EKF, and RLSTM-SGEKF models*

In this paper, a relevant attention mechanism is used as a data optimizer to ensure faster training times and fewer iterations than the traditional LSTM network for SOC estimation. Using a system with a processor: Intel (R) Core (TM) i5-3230M CPU @ 2.60GHz and a system type of 64-bit OS (x64-based processor), the training time (min and sec) for the SOC estimation by the LSTM and RLSTM networks under all three working conditions is presented based on the training and testing sequence. Due to the processing speed of the system with a single CPU, an epoch of 300 is selected. The sequence and time for the training and testing based on working conditions for both LSTM and RLSTM networks are presented in Table 3.

Table 3. The sequence and time for training and testing on a working condition basis for both LSTM and RLSTM networks for SOC estimation

Training working conditions	BBDST	DST	HPPC	BBDST	DST	HPPC	BBDST	DST	HPPC
Testing working conditions	BBDST	BBDST	BBDST	DST	DST	DST	HPPC	HPPC	HPPC
LSTM (min:ss)	216:35	338:26	678:11	210:21	425:08	769:40	217:29	421:79	854.19
RLSTM (min:ss)	27:48	54:49	44:19	31:52	70:14	35:42	24:49	49:18	32:45

In Table 3, the training working conditions row shows the working conditions from which the dataset is used to train the LSTM and RLSTM networks independently. Also, the testing working conditions row shows the working conditions from which the dataset is used for the SOC estimation. The training and testing times of the LSTM and RLSTM networks are presented in minutes. It can be observed that the RLSTM trains and tests much faster than the LSTM due to the proposed attention weights using the same hyperparameters.

In this study, the training times show that the LSTM network trains faster with datasets from the BBDST than with other working conditions, which is due to the size of the dataset. However, due to the working principle of the RLSTM network to select the relevant data during the training process, its training times do not depend on the size of the dataset, but they are subjective to the relevant attention mechanism. It can also be observed that the RLSTM trains the network faster than the traditional LSTM network, depending on the size and noise of the dataset encountered during the training process. Also, the RLSTM network does not depend on the processor speed of the training system or computer.

The validation and training state performances that initialize the training of the LSTM network and the training progress for the working condition-based SOC estimation are presented in Fig. 6.

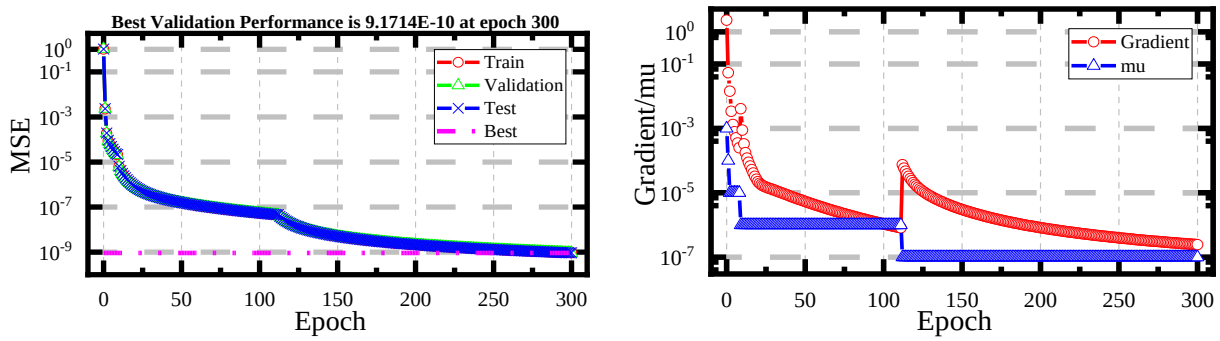

(a) Validation and training state performance curves

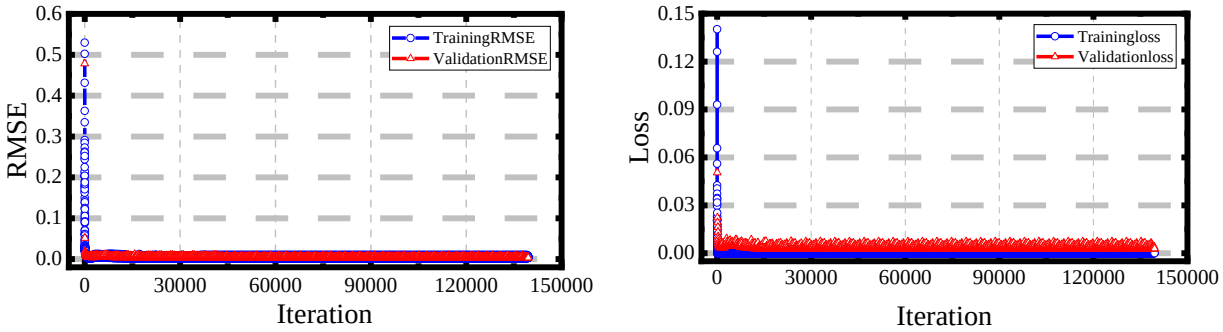

(b) Training progress RMSE and loss curves

Fig. 6. The LSTM-SOC network validation and training progress curves

Fig. 6 (a) shows the validation and training state performances of the parallel training pool. It shows the total number of epoch iterations and time taken to initiate the training with the performance using the LSTM network. Fig. 6 (b) shows the training RMSE and loss with the total iterations for the training of the LSTM network.

(a) *SOC estimation and performance evaluation of the working condition trained and tested LSTM network*

In this paper, tests are conducted to study the effects of the working conditions used for training and testing on the SOC estimation accuracy of the traditional LSTM network. This training and testing sequence is verified using three different experimental tests, namely BBDST, DST, and HPPC working conditions. The SOC estimation results using the LSTM network based on the training and testing sequence in Table 3 for the BBDST, DST, and HPPC working conditions are presented in Fig. 7.

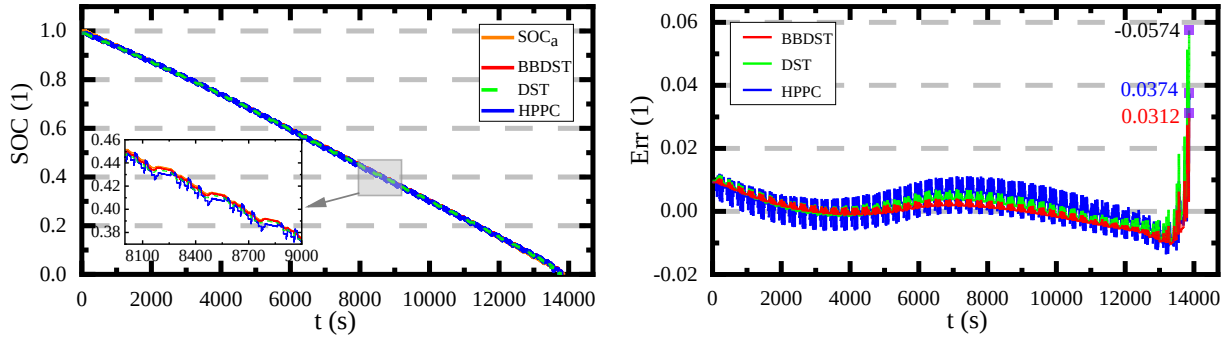

(i) SOC estimation curves (ii) Error curves

(a) SOC estimation tested under the BBDST and trained under the three working conditions

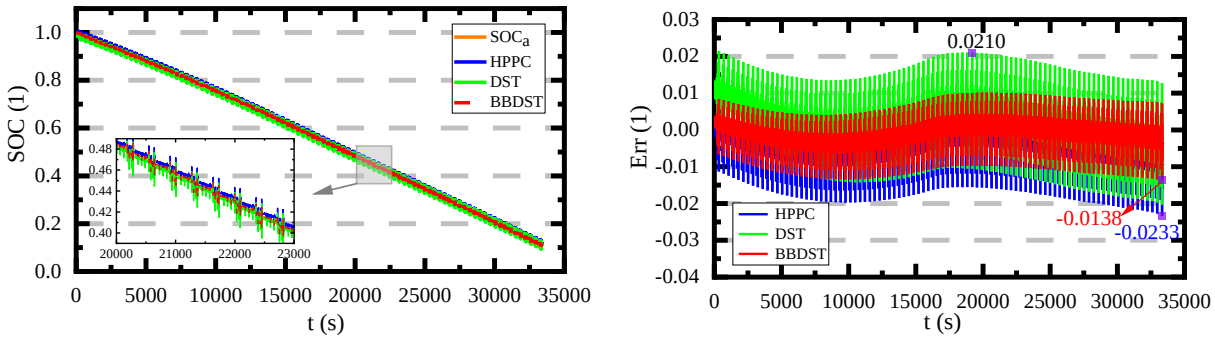

(i) SOC estimation curves (ii) Error curves

(b) SOC estimation tested under the DST and trained under the three working conditions

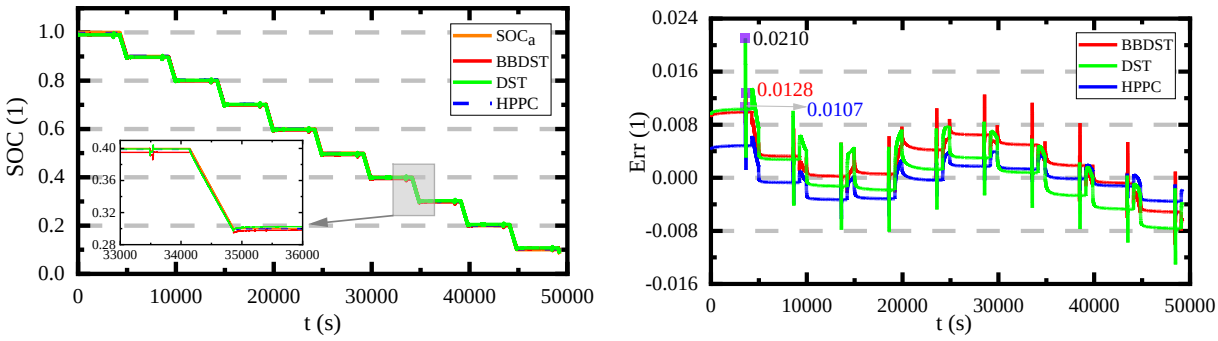

(i) SOC estimation curves (ii) Error curves

(c) SOC estimation tested under the HPPC and trained under the three working conditions

Fig. 7. SOC estimation tested under the BBDST, DST, and HPPC working conditions of the working condition trained and tested LSTM network

Fig. 7 shows the SOC estimation conducted based on the proposed training and testing technique under the BBDST, DST, and HPPC working conditions using the LSTM network. In the subfigures, SOC_a is the actual SOC of the battery system. The BBDST, DST, and HPPC are the SOC estimation results for the respective working conditions under which they are estimated or tested by the LSTM network.

In Fig. 7 (a), the SOC is estimated using a dataset from the BBDST working condition and trained using datasets from the BBDST, DST, and HPPC working conditions, respectively. For the respective training-testing sequence, the test results show that the ME for the BBDST-BBDST is 0.0312 (3.12%), the DST-BBDST is 0.0574 (5.74%), and the HPPC-BBDST is 0.0374 (3.74%). Also, it can be observed that the BBDST trained and tested result with an ME of 3.12% has the least noise fluctuations and has more stability than when it is trained under the DST and HPPC working conditions.

Also, in Fig. 7 (b), the SOC is estimated using a testing dataset from the DST working condition and trained using datasets from BBDST, DST, and HPPC working conditions, respectively. For this training and testing sequence, the DST has the second-lowest ME of 2.10%. The test results show that the ME for the BBDST-DST is 0.0138 (1.38%), the DST-DST is 0.0210 (2.10%), and the HPPC-DST is 0.0233 (2.33%). Under the DST working condition, it can be observed that all the estimation error results have the same noise effects, which is an inherent working condition effect.

Finally, Fig. 7 (c) shows the SOC estimated using a testing dataset from the HPPC working condition and trained using datasets from the BBDST, DST, and HPPC working conditions. The test results show that the ME for the BBDST-HPPC is 0.0128 (1.28%), the DST-HPPC is 0.0210 (2.10%), and the HPPC-HPPC is 0.0107 (1.07%). Also, it can be observed that the HPPC trained and tested result has more stability and less noise effect than when it is trained under the other working conditions with an ME of 1.07%.

Moreover, it can be observed that the LSTM network has a more optimal performance due to the accurate selection of the hyperparameter and also the training and testing technique proposed for this study. A summary of the MEs for the SOC estimation of the working condition-based training and testing technique using the LSTM network is presented in Table 4.

Table 4. The maximum error values of the working condition trained and tested LSTM network

Model	BBDST-BBDST	DST-BBDST	HPPC-BBDST	BBDST-DST	DST-DST	HPPC-DST	BBDST-HPPC	DST-HPPC	HPPC-HPPC
LSTM	3.12%	5.74%	3.74%	1.38%	2.10%	2.33%	1.28%	2.10%	1.07%

The performance evaluation of the SOC estimation results of the working condition-based training and testing technique using the LSTM network under the BBDST, DST, and HPPC working conditions are presented in Fig. 8.

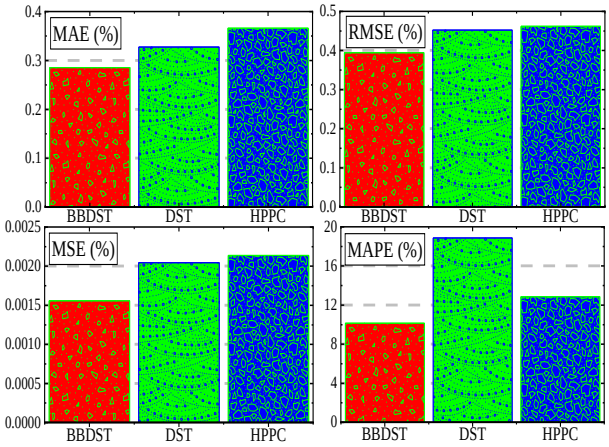

(a) Performance evaluation under the BBDST working condition

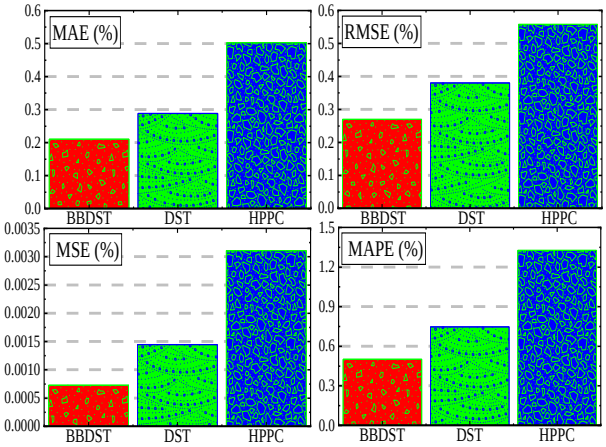

(b) Performance evaluation under the DST working condition

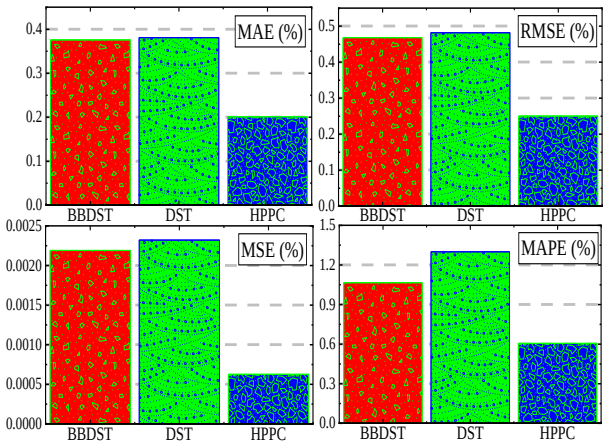

(c) Performance evaluation under the HPPC working condition

Fig. 8. Performance evaluation of the working condition trained and tested LSTM network

In Fig. 8 (a), the error results for the SOC estimation under the BBDST show that the BBDST-trained optimally performed more than when compared to the ones trained under the DST and HPPC working conditions. Also, the HPPC working condition-based SOC estimation has the optimal performance when trained and tested under the HPPC better than under the BBDST and DST working conditions, as presented in Fig. 8 (c). As presented in Fig. 8 (b), even though the performance of the network trained and tested under the DST is not optimal, its estimation error is closer to the minimum, which is the BBDST, than the HPPC working condition with the least accuracy.

These results verify that the accuracy of SOC estimation using the LSTM network is influenced by the working conditions under which it is trained and tested. Also, these estimation results show that the LSTM network used for this study performs better under the BBDST than under the other working conditions.

(b) *SOC estimation and performance evaluation of the RLSTM, RLSTM-EKF, and RLSTM-SGEKF models*

(i) *SOC estimation of the RLSTM, RLSTM-EKF, and RLSTM-SGEKF models*

The SOC estimation results of the RLSTM, RLSTM-EKF, and RLSTM-SGEKF models with the same training and testing sequence under the BBDST, DST, and HPPC working conditions are presented in Fig. 9.

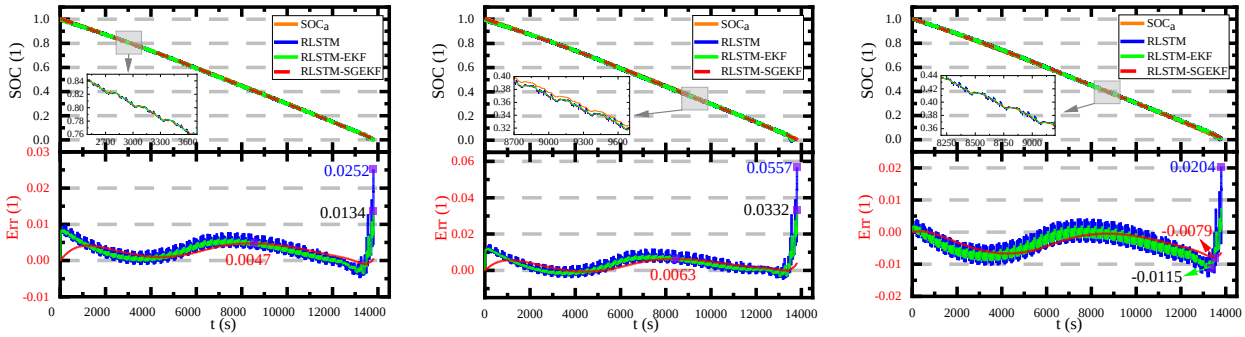

(i) BBDST-BBDST (ii) DST-BBDST (iii) HPPC-BBDST

(a) SOC estimation results under the BBDST working condition

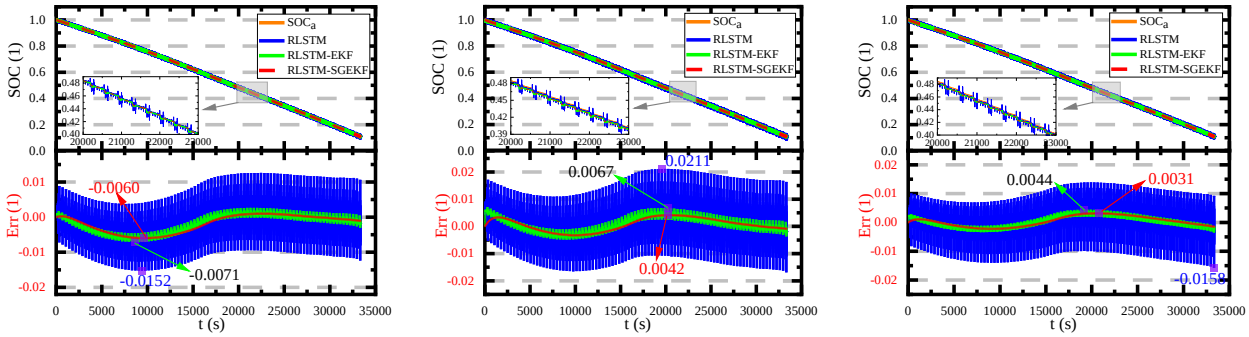

(i) BBDST-DST (ii) DST-DST (iii) HPPC-DST

(b) SOC estimation results under the DST working condition

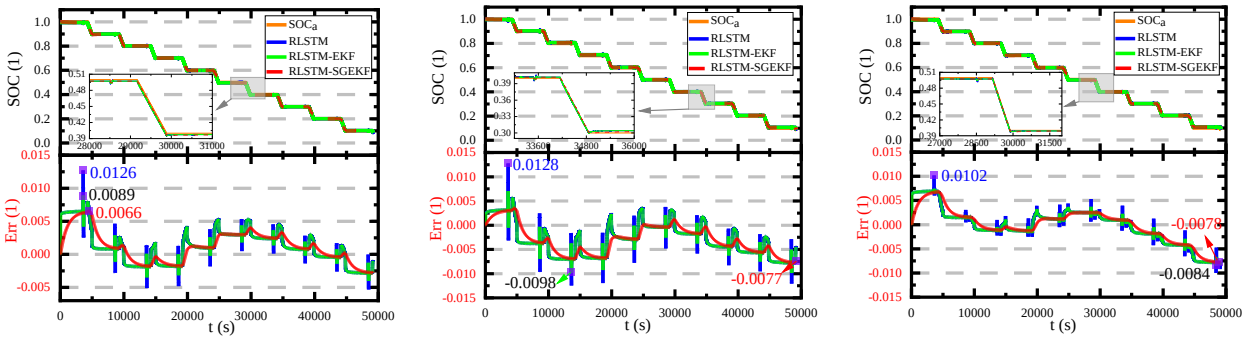

(i) BBDST-HPPC (ii) DST-HPPC (iii) HPPC-HPPC

(c) SOC estimation results under the HPPC working condition

Fig. 9. SOC estimation results of the RLSTM, RLSTM-EKF, and RLSTM-SGEKF models under the BBDST, DST, and HPPC working conditions

Fig. 9 shows the SOC estimation results of the RLSTM, RLSTM-EKF, and RLSTM-SGEKF models under the BBDST, DST, and HPPC working conditions based on the training and testing sequence to show the accuracy and robust performance for each enhanced model. It can be observed that the RLSTM-SGEKF model has better SOC initialization and adapts more quickly to the actual SOC with optimal accuracy than both the RLSTM network and the RLSTM-EKF model. Also, it further denoised the estimates of the previous models to ensure a steady-state SOC estimation with minimized MEs. During the estimation, it is observed that the RLSTM-SGEKF model has three (3) times faster convergence than the RLSTM-EKF model, which solves the convergence and speed issues essential in the SOC estimation of lithium-ion batteries to show its robustness, efficiency, and suitability for the online BMS application in real-time.

The ME values for the SOC estimation under the BBDST, DST, and HPPC working conditions using the same training and testing sequence are presented in Table 5.

Table 5. The maximum error values of the RLSTM, RLSTM-EKF, and RLSTM-SGEKF models

Models	BBDST-BBDST	DST-BBDST	HPPC-BBDST	BBDST-DST	DST-DST	HPPC-DST	BBDST-HPPC	DST-HPPC	HPPC-HPPC
RLSTM	2.52%	5.57%	2.04%	1.52%	2.11%	1.58%	1.26%	1.28%	1.02%
RLSTM-EKF	1.34%	3.32%	1.15%	0.71%	0.67%	0.44%	0.89%	0.98%	0.84%
RLSTM-SGEKF	0.47%	0.63%	0.79%	0.60%	0.42%	0.31%	0.66%	0.77%	0.78%

From Table 5, it can be observed that the RLSTM-SGEKF model has the optimal SOC estimation performance with the least ME values and enhanced robustness compared to the previous models under all the three working conditions.

(ii) *Performance evaluation of the RLSTM, RLSTM-EKF, and RLSTM-SGEKF models*

The error metrics are calculated to evaluate the performance of the RLSTM, RLSTM-EKF, and RLSTM-SGEKF models using the same training and testing sequence for the SOC estimation. The values of the MAE, MSE, RMSE, and MAPE of the RLSTM, RLSTM-EKF, and RLSTM-SGEKF models are graphically presented in Fig. 10.

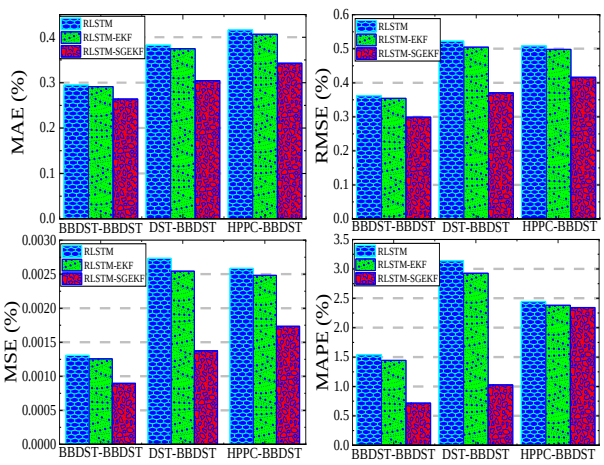

(a) Performance evaluation under the BBDST working condition

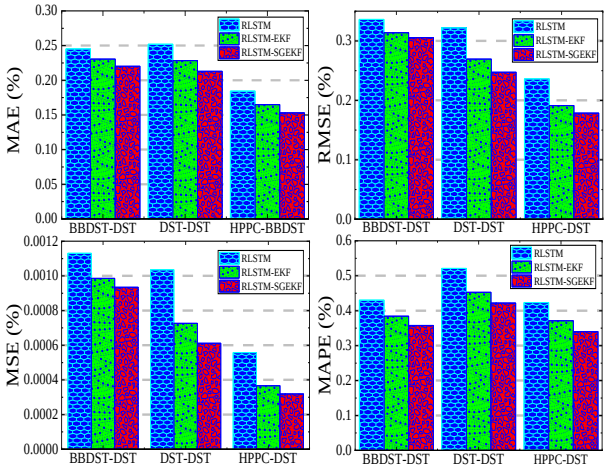

(b) Performance evaluation under the DST working condition

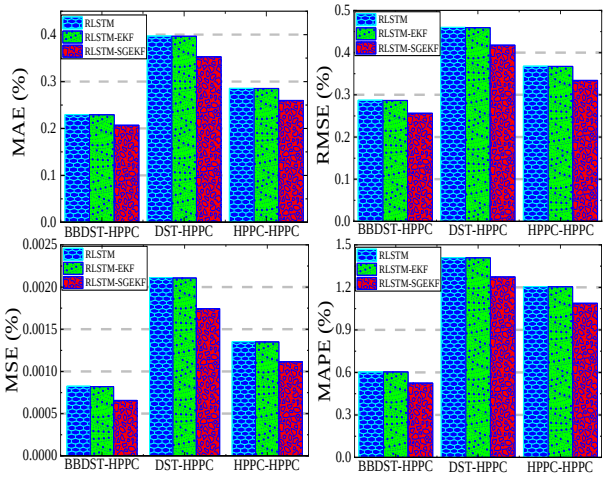

(c) Performance evaluation under the HPPC working condition

Fig. 10. Performance evaluation of the RLSTM, RLSTM-EKF, and RLSTM-SGEKF models under the BBDST, DST, and HPPC working conditions

In Fig. 10, the performance for each enhanced model is presented according to the working condition-based training and testing sequence. It can be observed that the RLSTM-SGEKF model has the least errors, while the errors of the RLSTM-EKF model and the RLSTM network increase accordingly. These error results show and verify the robustness and accuracy of the proposed hybrid models, the RLSTM-EKF and RLSTM-SGEKF models, over the data-driven models, the LSTM and RLSTM networks.

However, these results for these models are not evaluated based on the working condition training and testing technique to study their effect on the accuracy of the SOC estimation due to the infiltration by the data optimizer in the RLSTM network and the EKF method in the RLSTM-EKF and RLSTM-SGEKF models.

The maximum MAE, MSE, RMSE, and MAPE values for the LSTM, RLSTM, RLSTM-EKF, and RLSTM-SGEKF models under the BBDST, DST, and HPPC working conditions are calculated and presented in Table 6.

Table 6. The maximum MAE, MSE, RMSE, and MAPE values for the LSTM, RLSTM, RLSTM-EKF, and RLSTM-SGEKF models

Testing working condition	Models	MAE (%)	MSE (%)	RMSE (%)	MAPE (%)
BBDST	LSTM	0.36618	0.0021431	0.46225	12.85541
	RLSTM	0.41633	0.0027345	0.52284	3.13910
	RLSTM-EKF	0.40678	0.0025455	0.50464	2.92659
	RLSTM-SGEKF	0.34281	0.0017344	0.41639	2.34403
DST	LSTM	0.50279	0.0031110	0.55766	1.32640
	RLSTM	0.25202	0.0011302	0.33609	0.52113
	RLSTM-EKF	0.23047	0.0009856	0.31386	0.45274
	RLSTM-SGEKF	0.22016	0.0009346	0.30566	0.42178
HPPC	LSTM	0.38102	0.0023244	0.48175	1.30038
	RLSTM	0.39718	0.0021132	0.45970	1.41025

	RLSTM-EKF	0.39665	0.0021074	0.45903	1.40918
	RLSTM-SGEKF	0.35299	0.0017448	0.41765	1.27365

The results in Table 6 show that the RLSTM-SGEKF model has the optimal performance with minimum MAE, MSE, RMSE, and MAPE values under the three working conditions compared to the previous models. These results show the robustness, adaptability, and proficiency of the proposed hybrid model for the estimation of online SOC by the BMS for real-time EV applications.

4. Conclusion

In this paper, an LSTM network is established based on a working condition training and testing technique to study its effect on the accuracy of the SOC through a transfer learning technique. Three complex working conditions are used for the study based on the power and dynamic performance profiles of the lithium-ion battery, which are BBDST, DST, and HPPC. Secondly, a relevant attention mechanism is introduced as a data optimizer into the LSTM network for faster training to establish an RLSTM network. Thirdly, the SOC estimated by the RLSTM is input with the working current into the EKF and SGEKF methods to iteratively denoise and optimize the accuracy of the final SOC under the BBDST, DST, and HPPC working conditions. The results show that the working condition-based training and testing technique provides a criterion for accurate SOC estimation. Furthermore, the proposed RLSTM network has a more computationally efficient training time compared to the traditional LSTM network due to its attention weight. Finally, the SOC estimated results of the RLSTM-EKF and RLSTM-SGEKF models show that they are denoised and optimized to produce highly accurate estimates compared to the previous models. Moreover, the RLSTM-SGEKF model is optimal with maximum MAE, MSE, RMSE, and MAPE values of 0.34281%, 0.0017344%, 0.41639%, and 2.34403%, respectively, under the BBDST working condition. Under the DST working condition, the maximum MAE, MSE, RMSE, and MAPE values are 0.22016%, 0.0009346%, 0.30566%, and 0.42178%, respectively. Finally, under the HPPC working condition, the maximum MAE, MSE, RMSE, and MAPE values are 0.35299%, 0.0017448%, 0.41765%, and 1.27365%, respectively. These results show the suitability, robustness, and efficacy of the proposed hybrid models for the online SOC estimation of lithium-ion batteries by the BMS for real-time EV applications.

In our future work, we will focus on estimating the SOC and other state parameters using the RLSTM-SGEKF model under different temperatures and battery aging status to study their effects on the accuracy of the SOC of lithium-ion batteries.

Data availability

The authors declare that the main data supporting the findings of this study are available within the article and its supporting information files. Extra data are available from the authors on reasonable request: https://www.researchgate.net/project/Battery-life-test.

Declaration of competing interest

The authors declare no known competing financial interests or personal relationships that influence the work reported in this paper.

CrediT Author Statement

Paul Takyi-Aninakwa: Methodology, conceptualization, software, writing-original draft, analysis, data curation; **Shunli Wang**: Supervision, validation, resources; **Hongying Zhang**: Validation, resources, investigation; **Huan Li**: Software; **Wenhua Xu**: Writing and editing; **Carlos Fernandez**: Writing and editing

Acknowledgment

The work is supported by the National Natural Science Foundation of China (No. 61801407), China Scholarship Council (No. 201908515099), Fund of Robot Technology used for Special Environment Key Laboratory of Sichuan Province (No. 18kftk03), and Natural Science Foundation of Southwest University of Science and Technology (No.17zx7110, 18zx7145).

References

[1] Hannan M.A., Wali S.B., Ker P.J., Abd Rahman M.S., Mansor M., Ramachandaramurthy V.K., Muttaqi K.M., Mahlia T.M.I., Dong Z.Y., Battery energy-storage system: A review of technologies, optimization objectives, constraints, approaches, and outstanding issues, Journal of Energy Storage 42 (2021) 103023, https://doi.org/10.1016/j.est.2021.103023

[2] Espeda I.B., Jinasena A., Burheim O.S., Lamb J.J., Current trends for state-of-charge (SOC) estimation in lithium-Ion battery e lectric vehicles, Energies, 2021, 14(11), 3284, https://doi.org/10.3390/en14113284

[3] Liu F., Dai J., Equalization circuit topologies of lithium battery strings: a brief review, J. Phys.: Conf. Ser., 1633 (2020) 012141, https://doi:10.1088/1742-6596/1633/1/012141

[4] Ling L., Sun D., Yu X., Huang R., State of charge estimation of lithium-ion batteries based on the probabilistic fusion of two kinds of cubature Kalman filters, Journal of Energy Storage, 43, 2021, 103070, https://doi.org/10.1016/j.est.2021.103070

[5] Rzepka B., Bischof S., Blank T., Implementing an extended Kalman filter for SOC estimation of a li-ion battery with hysteresis: a step-by-step guide, Energies, 14(13), 2021, 3733, https://doi.org/10.3390/en14133733

[6] Duan J., Tang X., Dai H., Yang Y., Wu W., Wei X., Huang Y., Building safe lithium-ion batteries for electric vehicles: a review, Electrochem. Energ. Rev. 3, 1–42 (2020). https://doi.org/10.1007/s41918-019-00060-4

[7] Qu J., Liu F., Ma Y., Fan J., A neural-network-based method for RUL prediction and SOH monitoring of lithium-ion battery, IEEE Access, 2019, 7, 87178–87191

[8] Yang K., Tang Y., Zhang Z., Parameter identification and state-of-charge estimation for lithium-ion batteries using separated time scales and extended Kalman filter, Energies, 2021, 14, 1054. https://doi.org/10.3390/en14041054

[9] Keilz J., Jossen A., Electrochemical modeling of linear and nonlinear aging of lithium-ion cells, Journal of the Electrochemical Society, 167, 2020, 110535

[10] Shchurov N.I., Dedov S.I., Malozyomov B.V., Shtang A.A., Martyushev N.V., Klyuev R.V., Andriashin S.N., Degradation of lithium-ion batteries in an electric transport complex, Energies 2021, 14, 8072. https://doi.org/10.3390/en14238072

[11] Fath J.P., Dragicevic D., Bittel L., Nuhic A., Sieg J., Hahn S., Alsheimer L., Spier B., Wetzel T., Quantification of aging mechanisms and inhomogeneity in cycled lithium-ion cells by differential voltage analysis, Journal of Energy Storage 25, 2019, 16, 100813

[12] Lv J., Jiang B., Wang X., Liu Y., Fu Y., Estimation of the state of charge of lithium batteries based on adaptive unscented Kalman filter algorithm, Electronics, 2020, 9, 1425, https://doi:10.3390/electronics9091425
[13] Fan B., Luan X., Zhang R., Niu T., Xie Y., Research on SOC estimation algorithm for lithium battery based on EKF algorithm and ampere-hour integration method, 2nd International Conference on Electrical, Control, and Automation Engineering (ECAE), Advances in Engineering Research, 2018, 140, 101–105, https://doi.org/10.2991/ecae-17.2018.22
[14] Yu M., Li Y., Podlubny I., Gong F., Sun Y., Zhang Q., Shang Y., Duan B., Zhang C., Fractional-order modeling of lithium-ion batteries using additive noise assisted modeling and correlative information criterion, Journal of Advanced Research (2020), https://doi.org/10.1016/j.jare.2020.06.003
[15] Li W., Luo M., Tan Y., Cui X., Online parameters identification and state of charge estimation for lithium-ion battery using adaptive cubature Kalman filter, World Electr. Veh. J., 12, 2021, 123. https://doi.org/10.3390/wevj12030123
[16] Harding J.R., Han B., Madden S.B., Horn, Q.C., Examining the performance of implantable grade lithium-ion cells after over-discharge and thermally accelerated aging, Energies 2022, 15, 1405. https://doi.org/10.3390/en15041405
[17] Tian Y., Lai R., Li X., Xiang L., Tiana J., A combined method for state-of-charge estimation for lithium-ion batteries using a long short-term memory network and an adaptive cubature Kalman filter, Applied Energy 265 (2020) 114789, https://doi.org/10.1016/j.apenergy.2020.114789
[18] Yang X., Wang S., Xu W., Qiao J., Yu C. Takyi-Aninakwa P., Jin S., A novel fuzzy adaptive cubature Kalman filtering method for the state of charge and state of energy co-estimation of lithium-ion batteries, Electrochimica Acta 415, 2022, 140241, https://doi.org/10.1016/j.electacta.2022.140241
[19] Hannan M.A., Lipu M.S.H., Hussain A., Ker P.J., Mahlia T.M.I., Mansor M., Ayob A., Saad M.H., Dong Z.Y., Toward enhanced state of charge estimation of lithium-ion batteries using optimized machine learning techniques, Sci Rep 10, 4687 (2020). https://doi.org/10.1038/s41598-020-61464-7
[20] Prasad K.S.V., Divakar B.P., Real time estimation of SOC and SOH of batteries, International Journal of Renewable Energy Research, 8(1), 2018, 44–55
[21] Xin X., Wang S.L., Fernandez C., Yu C.M., Zou C.Y., Cong J., A novel practical state of charge estimation method: an adaptive improved ampere-hour method based on composite correction factor, Int J Energy Res. 2020;1–20, https://doi.org/10.1002/er.5758
[22] Movassagh K., Raihan A., Balasingam B., Pattipati K., Critical look at coulomb counting approach for state of charge estimation in batteries, Energies, 14, 2021, 4074. https://doi.org/10.3390/en14144074
[23] Zhang R., Xia B., Li B., Cao L., Lai Y., Zheng W., Wang H., Wang W., Wang M., A study on the open circuit voltage and state of charge characterization of high-capacity lithium-ion battery under different temperature, Energies 2018, 11, 2408; doi:10.3390/en11092408
[24] Tan Q., Gao Y., Liu K., Xu X., Sun Y., Yan P., A novel closed-loop control method for li-ion batteries connected in series power supply based on the time sequences recalculation algorithm. Symmetry, 2021, 13, 1463. https:// doi.org/10.3390/sym13081463
[25] Wang S., Fernandez C., Yu C., Fan Y., Cao W., Stroe D.-I., A novel charged state prediction method of the lithium-ion battery packs based on the composite equivalent modeling and improved splice Kalman filtering algorithm, Journal of Power Sources, 2020, 471, 228450, https://doi.org/10.1016/j.jpowsour.2020.228450
[26] Ge D., Zhang Z., Kong X., Wan Z., Online SoC estimation of lithium-ion batteries using a new sigma points Kalman filter, Appl. Sci. 2021, 11, 11797, p. 1-22, https://doi.org/10.3390/app112411797

[27] Komsiyska L., Buchberger T., Diehl S., Ehrensberger M., Hanzl C., Hartmann C., Hölzle M., Kleiner J., Lewerenz M., Liebhart B., Schmid M., Schneider D., Speer S., Stöttner J., Terbrack C., Hinterberger M., Endisch C., Critical review of intelligent battery systems: challenges, implementation, and potential for electric vehicles. Energies. 2021; 14(18):5989. https://doi.org/10.3390/en14185989
[28] Khaki B., Das P., An equivalent circuit model for vanadium redox batteries via hybrid extended Kalman filter and particle filter methods, Journal of Energy Storage 39 (2021) 102587, https://doi.org/10.1016/j.est.2021.102587
[29] Wang F.-K., Huang C.-Y., Mamo T., Ensemble model based on stacked long short-term memory model for cycle life prediction of lithium–ion batteries, Appl. Sci. 2020, 10, 3549, https://doi:10.3390/app10103549
[30] Cong J., Wang S., Wu B., Fernandez C., Xin X., Coffie-Ken J., A state-of-charge estimation method of the power lithium-ion battery in complex conditions based on adaptive square root extended Kalman filter, Energy, 2021, 219, 119603, https://doi.org/10.1016/j.energy.2020.119603
[31] Tian Y., Huang Z, Tian J., Li X., State of charge estimation of lithium-ion batteries based on cubature Kalman filters with different matrix decomposition strategies, Energy, 238, Part C, 1 January 2022, 121917, https://doi.org/10.1016/j.energy.2021.121917
[32] He L., Wang Y., Wei Y., Wang M., Hu X., Shi Q., An adaptive central difference Kalman filter approach for state of charge estimation by fractional order model of lithium-ion battery, Energy, 2021, 122627, https://doi.org/10.1016/j.energy.2021.122627
[33] Premkumar M., Kumar R.M., Karthick K., Sowmya R., SOC estimation and monitoring of Li-ion cell using Kalman-filter algorithm, Indonesian Journal of Electrical Engineering and Informatics (IJEEI), 6(4), 2018, 418–427, https://doi/10.11591/ijeei.v6i1.548
[34] Xu P., Li J., Sun C., Yang G., Sun F., Adaptive state-of-charge estimation for lithium-ion batteries by considering capacity degradation, Electronics, 2021, 10, 122, https://doi.org/10.3390/electronics10020122
[35] Azis N.A., Joelianto E., Widyotriatmo A., State of charge (SoC) and state of health (SoH) estimation of lithium-ion battery using dual extended Kalman filter based on polynomial battery model, 6th International Conference on Instrumentation, Control, and Automation (ICA), 2019, 8916734, 88–93, https://doi: 10.1109/ICA.2019.8916734
[36] Takyi-Aninakwa P., Wang S., Zhang H., Appiah E., Bobobee E.D., Fernandez C., A strong tracking adaptive fading-extended Kalman filter for the state of charge estimation of lithium-ion batteries. Int J Energy Res. 2022;1‐18. doi:10.1002/er.8307
[37] Fang L., Li J., Peng B., Online estimation and error analysis of both SOC and SOH of lithium-ion battery based on DEKF method, Energy Procedia, 158 (2019) 3008-3013, http://dx.doi.org/10.1016/j.egypro.2019.01.974
[38] Zhang S., Zhang X., A multi time-scale framework for state-of-charge and capacity estimation of lithium-ion battery under optimal operating temperature range, Journal of Energy Storage 35 (2021) 102325, https://doi.org/10.1016/j.est.2021.102325
[39] Zhang Z., Jiang L., Zhang L., Huang C., State-of-charge estimation of lithium-ion battery pack by using an adaptive extended Kalman filter for electric vehicles, Journal of Energy Storage, 37, 2021, 102457, https://doi.org/10.1016/j.est.2021.102457
[40] Chen Y., Xiong H., Guo Y., DEKF-based SOC estimation study for lithium batteries, Journal of Physics: Conference Series 2263 (2022) 012020, doi:10.1088/1742-6596/2263/1/012020

[41] Zeng M., Zhang P., Yang Y., Xie C., Shi Y., SOC and SOH joint estimation of the power batteries based on fuzzy unscented Kalman filtering algorithm, Energies, 2019, 12, 3122, 1–15, http://dx.doi.org/doi:10.3390/en12163122
[42] Guo X., Xu X., Geng J., Hua X., Gao Y., Liu Z., SOC estimation with an adaptive unscented Kalman filter based on model parameter optimization, Appl. Sci. 2019, 9, 4177; http://dx.doi.org/doi:10.3390/app9194177
[43] Lin X., Tang Y., Ren J., Wei Y., State of charge estimation with the adaptive unscented Kalman filter based on an accurate equivalent circuit model, Journal of Energy Storage, 41, 2021, 102840, https://doi.org/10.1016/j.est.2021.102840
[44] Chen Z., Sun H., Dong G., Wei J., Wu J., Particle filter-based state-of-charge estimation and remaining-dischargeable-time prediction method for lithium-ion batteries, Journal of Power Sources, 414, 2019, 158–166
[45] Ren P., Wang S., Huang J., Chen X., He M., Cao W., Novel co-estimation strategy based on forgetting factor dual particle filter algorithm for the state of charge and state of health of the lithium-ion battery, Int. J. Energy Res. 2021; 1- 14, https://doi.org/10.1002/er.7230
[46] Xu C., Zhang E., Yan S., Jiang K., Wang K., Wang Z., Cheng S., State of charge estimation for liquid metal battery based on an improved sliding mode observer, Journal of Energy Storage, 45, 2022, 103701, https://doi.org/10.1016/j.est.2021.103701
[47] Rezaei O., Moghaddam H. A., Papari B., A fast sliding-mode-based estimation of state-of-charge for Lithium-ion batteries for electric vehicle applications, Journal of Energy Storage, 45, 2022, 103484, https://doi.org/10.1016/j.est.2021.103484
[48] Chen Z., Zhou J., Zhou F., Xu S., State-of-charge estimation of lithium-ion batteries based on improved H infinity filter algorithm and its novel equalization method, Journal of Cleaner Production, 290, 2021, 125180, https://doi.org/10.1016/j.jclepro.2020.125180
[49] Dao V.Q., Dinh M.-C., Kim C.S., Park M., Doh C.-H., Bae J.H., Lee M.-K., Liu J., Bai Z., Design of an effective state of charge estimation method for a lithium-ion battery pack using extended Kalman filter and artificial neural network, Energies, 2021, 14(9), 2634 (1–20), https://doi.org/10.3390/en14092634
[50] Wang Y., Chen Z., A framework for state-of-charge and remaining discharge time prediction using unscented particle filter, Applied Energy, 260, 2020, 114324, https://doi.org/10.1016/j.apenergy.2019.114324
[51] Zhao L., Wang Y., Cheng J., A hybrid method for remaining useful life estimation of lithium-ion battery with regeneration phenomena, Appl. Sci. 2019, 9, 1890; doi:10.3390/app9091890
[52] Oyewole I., Chehade A., Kim Y., A controllable deep transfer learning network with multiple domain adaptation for battery state-of-charge estimation, Applied Energy, 312, (2022), 118726, https://doi.org/10.1016/j.apenergy.2022.118726
[53] Zhou W., Zheng Y., Pan Z., Lu Q., Review on the battery model and SOC estimation method, Processes 2021, 9, 1685. https://doi.org/10.3390/pr9091685
[54] Wang Z., Ma Q., Guo Y., Remaining useful life prediction of lithium-ion batteries based on deep learning and soft sensing, Actuators, 10, 2021, 234, https://doi.org/10.3390/act10090234
[55] Gou B., Xu Y., Feng X., State-of-health estimation and remaining-useful-life prediction for lithium-ion battery using a hybrid data-driven method, IEEE Transactions on Vehicular Technology, 69(10), 2020, 10854–10867, https://doi.org/10.1109/TVT.2020.3014932
[56] Wang S., Ren P., Takyi-Aninakwa P., Jin S., Fernandez C., A critical review of improved deep convolutional neural network for multi-timescale state prediction of lithium-ion batteries, Energies 2022, 15, 5053. https://doi.org/10.3390/en15145053

[57] Bonfitto A., Feraco S., Tonoli A., Amati N., Monti F., Estimation accuracy and computational cost analysis of artificial neural networks for the state of charge estimation in lithium batteries, Batteries, 2019, 5(2), 47, 1–17, https://dx.doi.org/10.3390/batteries5020047
[58] Zhang G., Xia B., Wang J., Intelligent state of charge estimation of lithium-ion batteries based on L-M optimized back-propagation neural network, Journal of Energy Storage, 44 (2021) 103442
[59] Feng X., Chen J., Zhang Z., Miao S., Zhu Q., State-of-charge estimation of lithium-ion battery based on clockwork recurrent neural network, Energy, 236, 2021, 121360, https://doi.org/10.1016/j.energy.2021.121360.
[60] Yang F., Li W., Li C., Miao Q., State-of-charge estimation of lithium-ion batteries based on gated recurrent neural network, Energy, 175, 2019, 66-75, https://doi.org/10.1016/j.energy.2019.03.059
[61] Ma L., Hu C., Cheng F., State of charge and state of energy estimation for lithium-ion batteries based on a long short-term memory neural network, Journal of Energy Storage, 37, 2021, 102440, https://doi.org/10.1016/j.est.2021.102440.
[62] Wei M., Ye M., Li J.B., Wang Q., Xu X., State of Charge Estimation of Lithium-Ion Batteries Using LSTM and NARX Neural Networks, IEEE Access, 8, 189236-189245, 2020, doi: 10.1109/ACCESS.2020.3031340
[63] Bian C., He H., Yang S., Stacked bidirectional long short-term memory networks for state-of-charge estimation of lithium-ion batteries, Energy, 191, 2020, 116538, https://doi.org/10.1016/j.energy.2019.116538
[64] Almaita E., Alshkoor S., Abdelsalam E., Almoman F., State of charge estimation for a group of lithium-ion batteries using long short-term memory neural network, Journal of Energy Storage 52 (2022) 104761, https://doi.org/10.1016/j.est.2022.104761
[65] Xi Z., Wang R., Fu Y., Mi C., Accurate and reliable state of charge estimation of lithium ion batteries using time-delayed recurrent neural networks through the identification of overexcited neurons, Applied Energy 305 (2022) 117962, https://doi.org/10.1016/j.apenergy.2021.117962
[66] Liu D., Li L., Song Y., Wu L., Peng Y., Hybrid state of charge estimation for lithium-ion battery under dynamic operating conditions, International Journal of Electrical Power & Energy Systems, 110, 2019, 48–61, https://doi.org/10.1016/j.ijepes.2019.02.046
[67] Lai X., Wang S., He L., Zhou L., Zheng Y., A hybrid state-of-charge estimation method based on credible increment for electric vehicle applications with large sensor and model errors, Journal of Energy Storage, 27, 2020, 101106, https://doi.org/10.1016/j.est.2019.101106
[68] Song X., Yang F., Wang D., Tsui K.-L., Combined CNN-LSTM network for state-of-charge estimation of lithium-ion batteries, IEEE Access, 2019, 7, 88894–88902
[69] Yang F., Zhang S., Li W., Miao Q., State-of-charge estimation of lithium-ion batteries using LSTM and UKF, Energy (2020), https://doi.org/10.1016/j.energy.2020.117664
[70] Fasahat M., Manthouri M., State of charge estimation of lithium-ion batteries using hybrid autoencoder and long short-term memory neural networks, Journal of Power Sources 469 (2020) 228375, https://doi.org/10.1016/j.jpowsour.2020.228375
[71] Shin D., Yoon B., Yoo S., Compensation method for estimating the state of charge of Li-polymer batteries using multiple long short-term memory networks based on the extended Kalman filter, Energies 14, 2021, 349 (1-19), https://doi.org/10.3390/en14020349
[72] Ren X., Liu S., Yu X., Dong X., A method for state-of-charge estimation of lithium-ion batteries based on PSO-LSTM, Energy, 234, 2021, 121236, https://doi.org/10.1016/j.energy.2021.121236

[73] Wang S., Takyi-Aninakwa P., Jin S., Yu C., Fernandez C., Stroe D.-I., An improved feedforward-long short-term memory modeling method for the whole-life-cycle state of charge prediction of lithium-ion batteries considering current-voltage-temperature variation, Energy, 254, Part A, 2022, 124224, https://doi.org/10.1016/j.energy.2022.124224
[74] Chen J., Zhang J., Xu X., Fu C., Zhang D., Zhang Q., Xuan Q., E-LSTM-D: A deep learning framework for dynamic network link prediction, IEEE Transactions on Systems, Man, and Cybernetics: Systems, 51, 6, 3699-3712, 2019, https://doi/10.1109/TSMC.2019.2932913
[75] Wang C., Lu N., Wang S., Cheng Y., Jiang B., Dynamic long short-term memory neural-network based indirect remaining-useful-life prognosis for satellite lithium-ion battery, Appl. Sci. 2018, 8, 2078, https://doi:10.3390/app8112078
[76] Ran X., Shan Z., Fang Y., Lin C., An LSTM-based method with attention mechanism for travel time prediction, Sensors 2019, 19, 861; doi:10.3390/s19040861
[77] Kingma D.P., Ba J.L., ADAM: a method for stochastic optimization, ICLR 2015, 1–15, arXiv:1412.6980v5 [cs. LG] 23 Apr 2015
[78] Kasai H., A MATLAB library for stochastic gradient descent algorithms, first version: June 20, 2018, 1–27, arXiv:1710.10951v2 [cs.MS] 18 Jun 2018
[79] Zhang S., Xu G., Zhang X., A novel one-way transmitted co-estimation framework for capacity and state-of-charge of lithium-ion battery based on double adaptive extended Kalman filters, Journal of Energy Storage, 2021, 33, 102093, https://doi.org/10.1016/j.est.2020.102093
[80] Wang S., Fan Y., Yu C., Jin S., Takyi-Aninakwa P., Fernandez C., Stroe D.-I., A novel collaborative multiscale weighting factor-adaptive Kalman filtering method for the time-varying whole-life-cycle state of charge estimation of lithium-ion batteries, Int J Energy Res. 2022; 46 (6): 7704–7721. doi:10.1002/er.7672